Environ. Sci. Technol. **2004**, *38,* 6590−6596

Phosphorus Immobilization in Micropores of Drinking-Water Treatment Residuals: Implications for Long-Term Stability

KONSTANTINOS C. MAKRIS,[†] WILLIE G. HARRIS,* GEORGE A. O'CONNOR, AND THOMAS A. OBREZA

Soil and Water Science Department, University of Florida, G163 McCarty Hall, P.O. Box 110290, University of Florida, Gainesville, Florida 32611

Drinking-water treatment residuals (WTRs) can immobilize excess soil phosphorus (P), but little is known about the long-term P retention by WTRs. To evaluate the long-term P sorption characteristics of one Fe- and one Al-based WTR, physicochemical properties pertinent to time-dependency and hysteresis of P sorption were assessed. This study also investigated the P sorption mechanisms that could affect the long-term stability of sorbed P by WTRs. Phosphorus sorption kinetics by the WTRs exhibited a slow phase that followed an initial rapid phase, as typically occurs with metal hydroxides. Phosphorus sorption maxima for both Fe- and Al-based WTRs exceeded 9100 mg of P kg^{-1} and required a greater specific surface area (SSA) than would be available based on BET-N_2 calculations. Electron microprobe analyses of cross-sectional, P-treated particles showed three-dimensional P sorption by WTRs. Carbon dioxide gas sorption was greater than N_2, suggesting steric restriction of N_2 diffusion by narrow micropore openings. Phosphorus-treated CO_2 SSAs were reduced by P treatment, suggesting P sorption by micropores (5−20 Å). Mercury intrusion porosimetry indicated negligible macroporosity (pores > 500 Å). Slow P sorption kinetics by WTRs may be explained by intraparticle P diffusion in micropores. Micropore-bound P should be stable and immobilized over long periods.

Introduction

Numerous studies have confirmed the close association between elevated P concentrations in water bodies and decreases in surface water quality. The source of P can be runoff and leaching from soils whose P sorption capacity is exceeded due to long-term applications of fertilizers, manures, and biosolids (*1*). Poorly P-sorbing soils are abundant in areas dominated by sandy soils, such as the coastal plain of the southeastern U.S. Low P sorbing capacities in conjunction with high water tables make these soils vulnerable to P losses (*2*).

Literature is abundant with studies that attempt to develop and demonstrate soluble P reduction techniques from wastewater (*3*), manure slurries (*4*), lakes (*5*), constructed wetlands (*6*), and soils amended with animal wastes (*7*). Most of the soluble P removal techniques are based on chemical immobilization of P with di- or trivalent metal salts. However, the cost associated with the use of metal salts may hinder their widespread use. Industrial byproducts high in Fe and/or Al content have been considered as cost-effective alternatives to metal salts to reduce soluble P in various media (*8*, *9*).

Recent studies have focused on the use of drinking-water treatment residuals (WTRs) as cost-effective materials to reduce soluble P in soils and runoff from areas amended with different P-sources (*10*−*16*), and in lake sediments (*5*). Drinking-WTRs are primarily amorphous Fe or Al hydroxides that also contain sediment, activated carbon, and polymers removed from the raw water produced during the water purification process (*17*). WTR reactivity is assumed to be similar to that of Al and Fe hydr(oxides). Land application could function as a means of WTRs disposal, and as a means of immobilizing P in poorly P-sorbing soils. The high amorphous Al or Fe content of the WTRs would be expected to increase a soil's P sorption capacity (*18*).

There are some limitations for WTRs use as P immobilizers. Drinking-water treatment plant facilities use different water sources and different coagulants. Thus, the WTRs produced have different physicochemical properties, and different sorption capacities. Dayton et al. (*19*) reported a range of P sorption capacities of 21 Al-WTRs tested in a field experiment. Other concerns include potential for induced plant P deficiencies when WTRs are over-applied (*20*), possible seasonal limitations in WTR availability, and uncertainty about the long-term stability of sorbed P.

Few data are available on the long-term P retention of WTRs or soils amended with WTRs or metal salts. To fully understand interactions between P and soil constituents, the effect of time needs to be considered (*21*). Phosphorus sorption kinetics by metal hydroxides and soils are well characterized and generally show a fast sorption phase followed by a slower reaction rate where sorption does not reach true equilibrium (*22*). The fast reaction is ascribed to low-energy external surface sites, where ligand exchange is believed to be the main adsorption mechanism (*22*). The slow reaction between P and metals with metal hydroxides proceeds for days or months and has been attributed to surface precipitation reactions (*23*, *24*), or intraparticle diffusion into micropores (*25*).

Surface precipitation has been envisioned to occur either above (*26*) or below (*27*) supersaturation with respect to the precipitating species. Ler and Stanforth (*28*) considered another type of surface precipitation where dissolution of the adsorbent provides a continuous supply of metals to precipitate with P in solution. This phosphate "burial" may result in decreased P availability with time. Metal-P precipitation would be favorable for long-term retention, especially if a stable crystalline metal-P phase were formed. Intraparticle diffusion of metal contaminants in metal hydroxides has well been documented (*25*). Diffusion-limited sorption in micropores was the rate-limiting step in Cu and Zn sorption by amorphous metal hydroxides during an "infinite bath" batch experiment (*25*).

Preliminary investigations of Fe- and Al-based WTRs revealed a discrepancy between macroscopic P sorption data and surface area available for P sorption based on N_2 specific surface area (N_2-SSA) measurements. In effect, the "external" SSA was insufficient to account for the quantity of sorbed P. This led to the hypothesis that P sorption on these WTRs was a three-dimensional process, accounting for the discrepancy

* Corresponding author phone: (352)392-1951, ext 251; fax: (352)-392-3902; e-mail: apatite@ufl.edu.

[†] Current address: Environmental Geochemistry Laboratory, Center for Water Research, University of Texas, San Antonio, 6900 North Loop 1604, San Antonio, TX 78249−0663. Telephone 210-458-5745 (work).

10.1021/es049161j CCC: $27.50
Published on Web 11/13/2004

between SSA and P sorption. The objectives of this study were to (i) document three-dimensional P distribution in WTR particles with duration of loading, and (ii) assess physiochemical properties of WTRs that elucidate P sorption mechanisms and their implications for stability of sorbed P.

Materials and Methods

WTRs Characterization. Two WTRs were used in this study: one Al- and one Fe-based. The Al-WTR was obtained from the Manatee Co. water treatment plant in Bradenton, FL. Additions of alum and a small amount of a copolymer of sodium acrylate and acrylamide produced the Al-WTR (Dr. McLeod, Bradenton Water Treatment facility, personal communication, 01/02). The Fe-WTR was obtained from the Hillsboro River water treatment plant in Tampa, FL, where $Fe_2(SO_4)_3$ was used as the coagulant. Both WTRs were sampled from stockpiles that were formed within a year since WTRs production.

The WTRs were air-dried and passed through a 2-mm sieve. The pH and soluble reactive P of the WTRs were measured in a 10 mM KCl solution at a 1:10 solid:solution ratio, after 40 d of equilibration. Total C and N were determined by combustion at 1010 °C using a Carlo-Erba NA-1500 CNS analyzer. The WTRs were analyzed for total-recoverable P, Fe, and Al by inductively coupled plasma-atomic emission spectroscopy (ICP-AES, Perkin-Elmer Plasma 3200) following digestion according to the EPA Method 3050B (*29*). The WTR particles were not completely dissolved by this procedure. Oxalate-extractable P, Fe, and Al were determined by ICP-AES after extraction at a 1:60 solid:solution ratio, following the procedures of McKeague et al. (*30*). Oxalate-extractable Fe and Al represent noncrystalline and organically complexed Fe and Al present in the solid (*30*). Phosphorus sorption kinetics and isotherms were performed at reaction intervals from 1 to 80 d as described by Makris (*31*). After completion of the sorption step, the supernatant was removed and WTR-containing tubes were filled with 5 mM oxalate solution (1:10 WTR:solution ratio). Suspensions reacted for 1, 10, 20, 40, and 80 d, without shaking or pH control.

Solid-State Characterization of WTRs. Following P desorption treatment, WTR particles were air-dried and subjected to solid-state characterization. Cross-sections for electron microscopy were prepared by embedding WTR particles in a low vapor pressure resin (Torr Seal, Varian) followed by mounting and polishing. Water-based mechanical polishing was performed using variable size silicon carbide abrasive papers (240−600 x). Surface microtopographic variability was minimized by examination of the particles under a microscope and repolishing until a flat surface was obtained. Samples were then carbon-coated to minimize charge localization. A cold-field emission scanning electron microscope coupled with an energy-dispersive X-ray spectrometer (SEM-EDS) was used to monitor P distribution in P-treated WTR particles.

For a more quantitative treatment, electron microprobe coupled with a wavelength-dispersive spectrometer (EPMA-WDS) was used to determine P distribution in polished cross sections of WTR particles, avoiding artificial cracks due to polishing. Measurements were made near the particle edges and within interior regions. The interior of the particles was designated ~60 μm on a straight-line distance away from the edge. The elemental composition of edges and interiors of untreated particles and particles treated with P for 1 and 80 d was determined to evaluate three-dimensional sorption and potential kinetic effects. Up to 15 particles per treatment were evaluated, and data were statistically analyzed. A completely randomized three-factorial design was used to compare differences between means of treatments at the 95% confidence interval, using the Design-Expert statistical software (*32*).

TABLE 1. General Chemical Properties of Two WTRs

source	pH	KCl-P (mg kg^{-1})	C (%)	N (%)	total (g kg^{-1}) P	total (g kg^{-1}) Fe	total (g kg^{-1}) Al	oxalate (g kg^{-1}) P	oxalate (g kg^{-1}) Fe	oxalate (g kg^{-1}) Al
Fe-WT R	6.3[a]	6.21	14.1	0.8	3.2	251	9.8	2.6	161	6.0
Al-WTR	5.4	5.08	16.2	0.6	3.1	6.2	92.4	2.98	5.2	91.1

[a] The results are the mean of two measurements.

Surface Area and Porosity. SSA characterization of the WTRs was performed before and after completion of the P sorption experiments (80 d). Particles were air-dried before being subjected to SSA determinations. SSAs of the WTRs were measured using N_2 and CO_2 as the adsorbates in a volumetric apparatus (Quantachrome Autosorb-1, Quantachrome Corp.). WTRs were outgassed in an He flow at 70 °C for 4 h. Di-nitrogen and CO_2 gas sorption experiments were performed in liquid N_2 (−196 °C), and ethylene glycol baths (0 °C), respectively, using a thermostat (Fisher Isotemp 3017). CO_2-based micropore volume and SSAs of the WTRs were calculated using the Dubinin−Radushkevich (DR) equation (*33*):

$$\log V = \log(V_0) - \frac{BT^2}{\beta}\left[\log\frac{P_0}{P}\right]^2 \quad (1)$$

V is the volume sorbed at standard pressure and temperature (cm^3 g^{-1}, STP), V_0 is the micropore capacity (cm^3 g^{-1}, STP), P_0 is the vapor saturation pressure of CO_2 (3.5 MPa), P is the equilibrium pressure (mmHg), B is a constant representing adsorption energy, and β is the affinity coefficient of CO_2 gas relative to P_0. The monolayer capacity V_0 is obtained by plotting log V against $[\log(P_0/P)]^2$.

The intercept of the linear plot is the monolayer micropore volume of CO_2 gas sorbed in micropores. The model assumes a Gaussian pore size distribution, and pore volume filling with the adsorbate. The degree of filling in micropores was a function of the negative differential free energy of adsorption. Micropore monolayer SSAs were calculated from the Dubinin−Radushkevich−Kawazoe (DRK) equation, which is a special case of the DR equation. The DRK equation assumes layer-by-layer gas sorption on the walls, and the only modification in eq 1 is that the amount of gas sorbed was used instead of the volume sorbed.

Mercury Intrusion Porosimetry. This technique uses a maximum pressure of ~410 Pa to intrude Hg into pores as small as ~1.8 nm (18 Å) and is usually applied for macroporous materials because it can quantify macropores up to 184 000 nm in diameter. The SSA was calculated by relating the total surface area of particles to the pressure−volume work required to force Hg into pores.

Results and Discussion

WTRs Properties. The two WTRs were acidic, with similar and relatively high C (*10*) and P contents (Table 1). They were representative of WTRs in composition (*34*), except that the Fe-WTR had higher total Fe content (251 g Fe kg^{-1}) than typical values reported in the literature. X-ray diffraction analysis (data not shown) verified the amorphous nature of both WTRs, with no apparent crystalline Fe and/or Al components. Phosphorus sorption experiments revealed large sorption capacities of both Al and Fe WTRs (*31*). In brief, the Fe-WTR sorbed nearly all of the P in solution (10 000 mg of P kg^{-1}), reaching 9100 mg of sorbed P kg^{-1}, after 80 d. The Al-WTR exhibited faster P sorption kinetics and sorbed essentially all P from solution within 10 d. Results from single-day P sorption experiments showed that the Fe-WTR sorbed

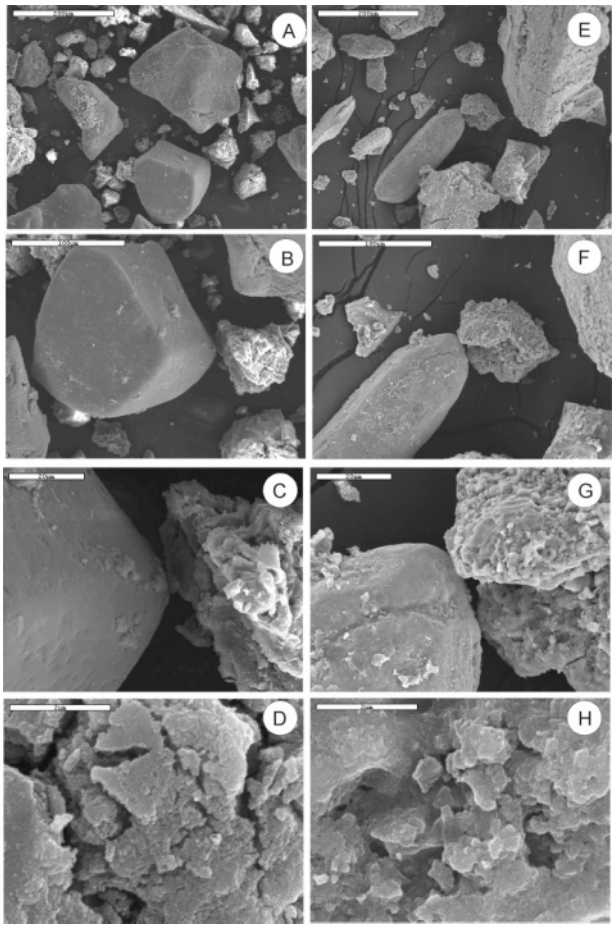

FIGURE 1. Scanning electron secondary images of the Al- and Fe-based WTRs. (A) Secondary image of representative Al-WTR particles; scale bar = 200 μm. (B) Magnified secondary image of a portion of image A; scale bar = 100 μm. (C) Secondary image of representative Al-WTR surfaces; rough and smooth surfaces; scale bar = 20 μm. (D) Magnified secondary image of the rough surface of the Al-WTR particle from image C; scale bar = 2 μm. (E) Secondary image of representative Fe-WTR particles; scale bar = 200 μm. (F) Magnified secondary image of a portion of image E; scale bar = 100 μm. (G) Secondary image of representative Fe-WTR surfaces; rough and smooth surfaces; scale bar = 20 μm. (H) Magnified secondary image of the rough surface of the Fe-WTR particle from image G; scale bar = 2 μm. Images D and H show surface porosity, but magnification is not large enough to show microporosity.

2000 mg of P kg^{-1} and the Al-WTR 7700 mg of P kg^{-1}. The affinity for P and relatively slow P sorption kinetics of the WTRs led us to suspect a sorption mechanism other than ligand exchange with structural hydroxyls on particle exterior surfaces.

Solid-State Characterization. Scanning electron secondary images showed similar particle morphology for both untreated WTRs (Figure 1). Images showed the irregular shape and variable size of WTR particles. Particle surfaces ranged from rough to fairly smooth. Elemental spectra (SEM-EDS) verified the presence of P, Al, and Fe, as well as Si, Ca, and Na. SEM-EDS dot maps of whole particles showed relatively uniform elemental distributions for both untreated (no P added) and P-treated samples (data not shown). The P in untreated WTRs comes from the original raw drinking water. Similar uniform P distribution, but greater dot intensity, was also observed for P-treated whole particles after 80 d. Bertrand et al. (*35*) used secondary ion mass spectrometry (SIMS) on goethite and calcite loaded with 2950 and 930 mg of P kg^{-1}, respectively, to study the association of P with the minerals. SIMS analysis, coupled with image analysis, showed that P

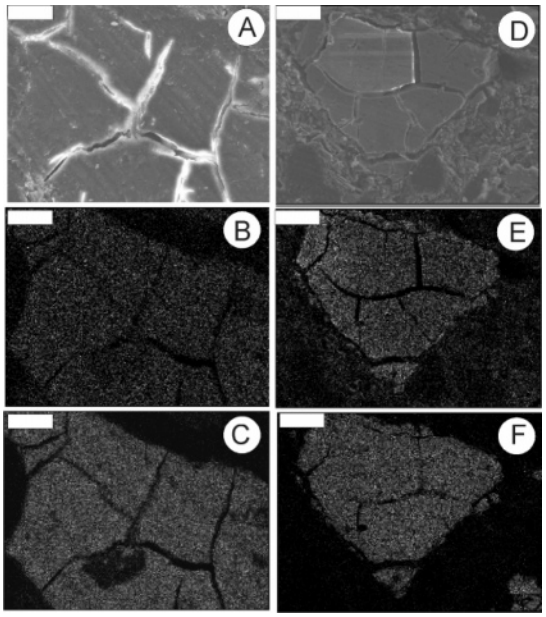

FIGURE 2. Scanning electron secondary images (A, D) and the corresponding P and metal dot maps (B, C, E, and F) of flat cross-sections after 80 d P treatment for both WTRs. (A) Secondary image of a representative Al-WTR cross-section; scale bar = 20 μm. (B) P dot map of the secondary image in (A). (C) Al dot map of the secondary image in (A). (D) Secondary image of a representative Fe-WTR cross-section; scale bar = 20 μm. (E) P dot map of the secondary image in (D). (F) Fe dot map of the secondary image in (D). Phosphorus dot maps of cross-sections for both WTRs show uniform P distribution, without evident surface precipitation of P. However, some P-treated Fe-WTR particles showed zonal P enrichment near the particle edge.

was evenly distributed on the goethite surface, but clustered on the calcite, suggesting adsorption for the former and precipitation for the latter.

Some data from studies utilizing high P loads and increased equilibration times of P-treated amorphous/poorly crystalline metal hydroxides support a P surface precipitation mechanism. Martin et al. (*36*) studied the slow P (1 mM KH_2PO_4) sorption by goethite. No solid-state P diffusion was suggested, but rather a metal-P surface precipitate. Nooney et al. (*24*) studied the slow P sorption by hematite and alumina by Auger electron spectroscopy and atomic force microscopy. After the first 10 min of hematite exposure to 120 mg of P L^{-1}, phosphate species precipitated as islands. The onset of three-dimensional island growth (surface localized precipitation) was at 1500−2000 min for the alumina surface.

No discrete surficial metal-P phases were detected in whole WTR particles with SEM-EDS spectroscopy, and we hypothesized that P diffuses into particles to reach meso- and micropore domains. SEM-EDS dot maps of cross-sections from both WTRs qualitatively supported an intraparticle sorption mechanism, showing that P was evenly distributed within the particles (Figure 2), except for some near-edge P zonation in Fe-WTR particles after P treatment. Cabrera et al. (*37*) suggested that slow P reaction with lepidocrocite was due to micropores within a network of connected crystals, which resulted in time-dependent P diffusion to distant sorption sites. Torrent et al. (*38*) suggested oxalate (200 mM)-extractable Fe and microporosity as the main factors that influenced slow P sorption by goethites.

EPMA-WDS analysis, which can be useful in assessing P distribution in soils (*39*−*42*), supported intraparticle P diffusion more quantitatively. Cross-sectional P distribution analysis of the P-treated WTRs showed significant ($p < 0.001$) increases in the relative P concentrations in the interior of

TABLE 2. Changes in Mean Relative P Concentrations (P/P + Fe) at the Edge and Interior (~60 μm Away from Edge) of Fe-WTR Particles with P Load (10 g P kg^{-1} Initial Load) and Time (1 and 80 d)[a]

	relative P concentration means P/(P + Fe)		
location	untreated	P-treated (1 d)	P-treated (80 d)
edge	0.008a	0.017b	0.020b
interior	0.009a	0.011a	0.016b

[a] As determined by electron microprobe of flat cross-sections. The untreated (no P) WTRs contain some P that came from the raw water. Different letters in columns and rows indicate statistical significance ($\alpha = 0.05$). Data indicate P movement to the interior of particles with time. Similar trends were observed for the Al-WTR.

TABLE 3. BET-N_2 SSAs, Total Micropore Volume, and CO_2-SSA Calculations Based on the Dubinin Radushkevich Method (DR) of the WTRs Treated with and without P for 80 d[a]

WTRs	treatment	BET-N_2 SSA (m^2 g^{-1})	Hg-based SSA (m^2 g^{-1})	DR micropore SSA (m^2 g^{-1})	total micropore volume (cm^3 g^{-1})
Fe-WTR	no P	3.9	2.5	27.5	0.012
	with P	2.9	nd[b]	17.3	0.008
Al-WTR	no P	36	33	104.9	0.042
	with P	27	nd	79.9	0.034

[a] A total of eight points were used for the linear regressions to calculate the DR micropore CO_2-based SSAs, and the r^2 values were 0.99 for all treatments. Numbers are the average of two replicates. [b] Not determined.

the particles (~60 μm inside) with time (from 1 to 80 d) (Table 2). The average P concentrations for P-treated particles (80 d) were slightly greater near the edge, but edge-versus-interior differences were not statistically different at the 95% confidence level (Table 2). Data for the Al-WTR were similar (not shown). Ippolito et al. (*43*) used EPMA-WDS dot maps to assess P distribution in a P-treated Al-WTR equilibrated for 211 d. Dot maps showed no evidence for P surface precipitation, but a uniform amorphous Al−P association throughout the particles (*43*).

EPMA-WDS data suggested that P moves in a three-dimensional fashion toward the interior of the WTR particles rather than accumulating significantly at the particle surface as by precipitation. This form of sorption may have favorable implications for P immobilization. Phosphorus desorption experiments with a 5 mM oxalate solution showed that P desorption was minimal for both WTRs (<1% sorbed P). Strauss et al. (*44*) conducted P desorption experiments after loading goethites with P. Minimal P desorption was proposed by these authors to be associated with a micropore diffusion mechanism, but they did not determine pore size distributions or SSAs.

Mercury Intrusion Porosimetry. WTRs were subjected to Hg intrusion porosimetry to assess the macroporosity of the materials (Table 3). We hypothesized that macro- and mesopores facilitated P intrusion of the WTR particles. BET-N_2 analysis is not capable of measuring macropores (>500 Å). Mercury porosimetry revealed a low volume of macropores for both WTRs; most of the pore volume accessed by Hg was in the pore size range of mesopores (20−500 Å, or 2−50 nm) (Figure 3). The total pore volume intruded by Hg for the Fe-WTR was very low. Hg intrusion-based SSA of the Fe-WTR was also low (~2.5 m^2 g^{-1}), and close to the value measured by the BET-N_2 method (3.9 m^2 g^{-1}). Similarly, Hg intrusion-based SSA of the Al-WTR (33 m^2 g^{-1}) was very close to the BET-N_2 SSA value (36 m^2 g^{-1}) (Table 3). Mercury porosimetry data show that both materials lack a significant network of macropores.

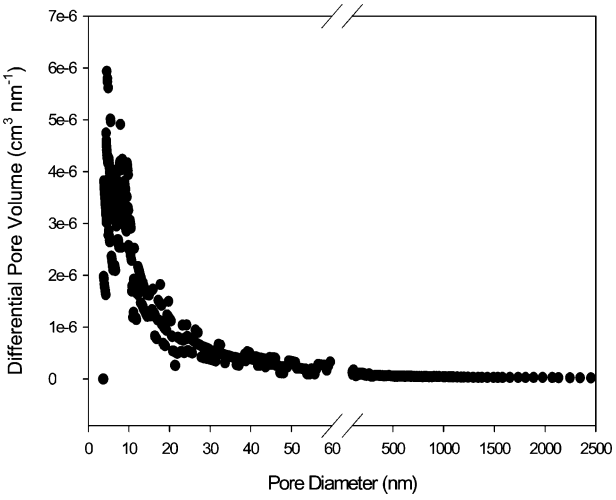

FIGURE 3. Differential Hg porosimetry-based pore volume distribution of the Fe-WTR. Lower macropore size limit is 50 nm (500 Å), based on the IUPAC classification. Data for Al-WTR were similar.

TABLE 4. Phosphate Parking Densities (PO_4 molecules nm^{-2}) at Different Sorption Times Based on N_2 and CO_2 SSA Measurements[a]

	based on N_2		based on CO_2	
	1 d	80 d	1 d	80 d
Fe-WTR	9.7	43.7	1.4	6.2
Al-WTR	4.2	5.4	1.4	1.9

[a] Densities based on N_2 exceed values calculated from reported short-term (1 d) densities for goethite (1.6 PO_4 molecules nm^{-2}) and gibbsite (0.6 PO_4 molecules nm^{-2}) (*23, 43*).

Micropore Surface Areas of the WTRs. We tested the hypothesis that P sorbed by WTRs resides mostly in micropores that originated during WTRs formation. The BET-N_2 SSA value of 3.9 m^2 g^{-1} for the Fe-WTR was lower than expected given the amorphous nature of this material (Table 3). However, repeated SSA measurements resulted in similar values even under different outgassing times and temperatures (data not shown). Assuming ligand exchange to be the predominant P adsorption mechanism during short-term P sorption (1 d), the Fe-WTR short-term (1 d) P adsorption density (1.7×10^{-5} mol of P m^{-2}) was reasonably close to the value reported by Tamura et al. (*45*). However, the Al-WTR short-term P adsorption density (6.8×10^{-6} mol of P m^{-2}) was lower, consistent with its greater BET-N_2 SSA. Total P uptake (80 d) was greater than the short-term P adsorption densities, that is, 1.0×10^{-4} and 1.2×10^{-5} mol of P m^{-2} for the Fe- and Al-WTR, respectively.

Mean P adsorption densities of goethites varying in crystallinity and SSAs after single day sorption at pH 6 were 2.6×10^{-6} mol of P m^{-2} (*43*), and 1.0×10^{-6} mol of P m^{-2} for gibbsites (*23*). A goethite with SSA similar to the Fe-WTR had a P adsorption (1 d) density of 2.9×10^{-6} mol of P m^{-2} (*38*). We calculated the parking density of PO_4 molecules, based on BET-N_2 SSA, as follows:

$$\text{parking density (no. of } PO_4 \text{ molecules } m^2) = S_{max} \times \text{Avogadro's no.} \quad (2)$$

where S_{max} is the apparent (1 d) adsorption capacity in moles of PO_4 m^{-2}.

Phosphate parking densities after 1 and 80 d were greater than the maximum density possible for the Fe-WTR (Table 4), considering a phosphate ionic radius of 0.22 nm. Densities were geometrically possible for the Al-WTR, but probably

were unrealistically high given other steric and electrostatic constraints. Furthermore, densities based on N_2 SSA were much greater for both WTRs than those calculated for crystalline Fe- and Al oxides (*23*, *38*, *43*) (Table 4).

Typically, adsorption is considered to be exothermic in nature and increases as temperature decreases. Sorption in narrow pores (micropores or bottleneck-shaped mesopores) may be diffusion-controlled and endothermic, involving significant amounts of activation energy. Apparent underestimation of SSAs via BET-N_2 suggests that N_2 molecules do not have the necessary activation energy to overcome energy barriers associated with micropores that might be present in the WTRs.

Instead of N_2, CO_2 has been used as the adsorbate for calculating micropore volume and specific surface areas (SSAs) of carbon molecular sieves and activated carbons (*46*, *47*), clay minerals (*48*), and soil organic matter (*49*). CO_2 has molecular dimensions similar to N_2 (3.0 Å for N_2 versus 2.8 Å for CO_2), but elevated temperatures (−196 °C for N_2, versus 0 °C for CO_2) and higher absolute pressures (N_2 vapor saturation pressure is 0.1 MPa, versus 3.5 MPa for CO_2) that are in effect during the CO_2-SSA analysis facilitate the access of micropores by CO_2 molecules (*50*). CO_2-SSA analysis, based on the DRK method (*51*), yielded greater SSAs than obtained by BET-N_2 and revealed that SSAs of both WTRs decreased with P treatment (Table 3). There was a similar decrease in the micropore volume of the P-treated WTRs, suggesting that sorbed phosphate blocks micropores. A similar trend in SSAs (N_2 < CO_2) for microporous activated carbons was explained as either restricted N_2 diffusion or narrow microporosity (*50*). Parking densities calculated from CO_2 SSA values were lower and more realistic than those calculated on the basis of BET-N_2 SSA (Table 4).

Chemical heterogeneity of WTRs, coupled with wide particle/pore size distributions, would affect the accuracy of determinations serving as the basis for these parking density comparisons. Near-surface characteristics (surface roughness and hydrophobicity) can influence N_2 and CO_2 gas sorption under dry conditions used in BET measurements (*53*). However, sorption of a polar hydrophilic molecule, like phosphate, is less likely to be affected by these characteristics than sorption of nonpolar organic compounds (*54*).

Uncertainty associated with estimating P adsorption capacities of the WTRs (fast reaction) could confound the comparison as well. The amount of P adsorbed in 1 day was used to calculate the amount of P required to complete a monolayer on the external surface of the WTRs (*23*, *38*). Single day P sorption, however, may not represent the time needed to form a complete monolayer on the WTR surface, and the time necessary may vary for WTRs with different physicochemical properties.

A grand canonical Monte Carlo computer simulation model was used to calculate the micropore (CO_2-based isotherm) volume distribution of the Fe-WTR (Figure 4). The model represents the pore structure of the WTR as a collection of slit-shaped pores with smooth graphite walls (*52*). Phosphate sorption in micropores shifted the micropore size distribution to larger size micropores possibly because phosphate occupied micropores ranging 4−8 Å (Figure 4). These SSA values represent only the surface area associated with pores up to 15 Å. Another line of evidence for microporosity of WTRs was found from isothermal (70 °C) thermogravimetric weight losses of both WTRs. Isothermal weight losses were time-dependent, suggesting the presence of micropore-bound water (data not shown).

Implications for Long-Term Stability. Phosphate molecules may reside in micropores (<15 Å) that are inaccessible by traditional BET-N_2 SSA measurements. Bottleneck-shaped micropores could limit P diffusion rates, being consistent with time-dependent P sorption and hysteretic desorption.

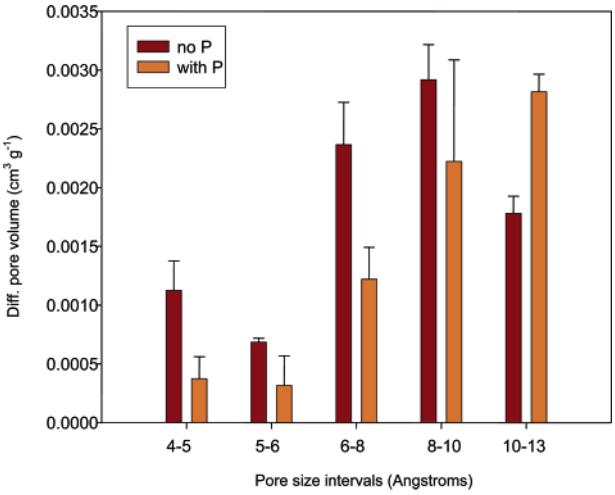

FIGURE 4. Pore size distribution of the Fe-WTR treated and untreated with P (10 g kg^{-1}) for 80 d, based on a grand canonical Monte Carlo model, using the CO_2 gas adsorption data. Error bars denote one standard deviation of replicated ($n = 2$) measurements.

Micropore-bound P likely resists desorption, which favors long-term stability of sorbed P by WTRs. Phosphorus desorption from WTRs was minimal (0.2% and 0.8 % of sorbed P). The limited P desorption likely reflects increased micropore energy potentials of pore walls and sorbed P. Micropore walls maximized bonding interaction between sorbent and sorbate, thus reducing sorbate availability. Phosphorus desorption likely occurs only when increasing amounts of activation energy are supplied to overcome energetic barriers associated with micropores. Micropores exhibit significantly greater interaction potentials than meso- or macropores or open surfaces (*55*) due to wall proximity.

Several studies have attempted to explain slow P sorption by metal hydroxides using the microporosity concept (*37*, *56*, *57*). All of these studies suggested a mechanism of P diffusion in micropores, but with no direct evidence such as is presented in this study. Micropore-bound P should not be released in circumneutral pH aqueous media. WTR particles maintained structural integrity for 160 d at pH 5−7, as monitored by soluble P and metal (Fe and Al) measurements in 10 mM KCl (data not shown).

Further studies are needed to predict the time scales over which P will be stable and immobilized by WTRs. A combination of diffusional and thermodynamic models might be required for such complex materials. Nonlinear fits of long-term P sorption kinetics data of the Fe-WTR to a diffusion model resulted in calculated a P diffusion coefficient on the order of 10^{-15} cm^2 s^{-1} (*31*), which is in accordance with slow diffusion in microporous sorbents (*25*). Estimated P concentrations after 80 d of reaction, 60 μm inside the particle measured with EPMA-WDS, were equal to 94% of predicted values from the diffusion model and the calculated P diffusion coefficient. However, the diffusion model was an idealized case where particles have a specific shape (spheres), and unimodal particle and pore size distributions. The model also assumed similar sorption/desorption reaction rates, ignoring hysteretic effects. Phosphorus diffusion coefficients will likely vary with WTR physicochemical properties, which would affect the ease with which P diffuses into the particle.

Our data suggest that P sorption is practically irreversible for the two WTRs, barring disintegration of the particles themselves. Our findings provide evidence to support the long-term stability of sorbed P by Fe- and Al-based WTRs, when land-applied to P-sensitive ecosystems. We are currently looking at other WTRs varying in physicochemical properties to determine long-term P retention characteristics.

Acknowledgments

We acknowledge U.S. EPA funding through Project CP-82963801. We also acknowledge the valuable contribution of Wayne A. Acree and the Major Analytical Instrumentation Center at the University of Florida to SEM-EDS and EMPA-WDS work. Contribution of the Florida Agricultural Experimental Station Journal Series No. R-10280.

Literature Cited

(1) Sharpley, A. N.; Daniel, T.; Sims, J. T.; Lemunyon, J.; Stevens, R.; Parry, R. *Agricultural Phosphorus and Eutrophication*; U.S. Department of Agriculture, U.S. GPO: Washington, DC, 1999.

(2) He, Z. L.; Alva, A. K.; Li, Y. C.; Calvert, D. V.; Banks, D. J. Sorption−desorption and solution concentration of phosphorus in a fertilized sandy soil. *J. Environ. Qual.* **1999**, *28*, 1804−1810.

(3) Omoike, A. I.; Vanloon, G. W. Removal of phosphorus and organic matter removal by alum during wastewater treatment. *Water Res.* **1999**, *33*, 3617−3627.

(4) Burns, R. T.; Moody, L. B.; Walker, F. R.; Raman, D. R. Laboratory and in-situ reductions of soluble phosphorus in swine waste slurries. *Environ. Technol.* **2001**, *22*, 1273−1278.

(5) Hoge, V. R.; Conrow, R.; Coveney, M.; Peterson, J. The application of alum residual as a phosphorus abatement tool within the lake Apopka restoration area. *WEF Proceedings Conference*, Alexandria, VA, 2003.

(6) Ann, Y.; Reddy, K. R.; Delfino, J. J. Influence of chemical amendments on phosphorus immobilization in soils from a constructed wetland. *Ecol. Eng.* **2000**, *14*, 157−167.

(7) Anderson, D. L.; Tuovinen, O. H.; Faber, A.; Ostrokowski, I. Use of soil amendments to reduce soluble phosphorus in dairy soils. *Ecol. Eng.* **1995**, *5*, 229−246.

(8) Codling, E. E.; Chaney, R. L.; Mulchi, C. L. Use of aluminum and iron-rich residues to immobilize phosphorus in poultry litter and litter-amended soils. *J. Environ. Qual.* **2000**, *29*, 1924−1931.

(9) Dao, T. H. Coamendments to modify phosphorus extractability and nitrogen/ phosphorus ratio in feedlot manure and composted manure. *J. Environ. Qual.* **1999**, *28*, 1114−1121.

(10) O'Connor, G. A.; Elliott, H. A. *Co-application of biosolids and water treatment residuals*; Final Report. Florida Department of Environmental Protection: Tallahassee, FL, 2000.

(11) O'Connor, G. A.; Elliott, H. A.; Lu, P. Characterizing water treatment residuals phosphorus retention. *Soil Crop Sci. Soc. Fla., Proc.* **2001**, *61*, 67−73.

(12) Elliott, H. A.; O'Connor, G. A.; Brinton, S. Phosphorus leaching from biosolids-amended sandy soils. *J. Environ. Qual.* **2002**, *31*, 1362−1369.

(13) Elliott, H. A.; O'Connor, G. A.; Lu, P.; Brinton, S. Influence of water treatment residuals on phosphorus solubility and leaching. *J. Environ. Qual.* **2002**, *31*, 681−689.

(14) Haustein, G. K.; Daniel, T. C.; Miller, D. M.; Moore, P. A., Jr.; Mcnew, R. W. Aluminum-containing residuals influence high-phosphorus soils and runoff water quality. *J. Environ. Qual.* **2000**, *29*, 1954−1959.

(15) Ippolito, J. A.; Barbarick, K. A.; Redente, E. F. Co-application of water treatment residuals and biosolids on two range grasses. *J. Environ. Qual.* **1999**, *28*, 1644−1650.

(16) Gallimore, L. E.; Basta, N. T.; Storm, D. E.; Payton, M. E.; Huhnke, R. H.; Smolen, M. D. Water treatment residual to reduce nutrients in surface runoff from agricultural land. *J. Environ. Qual.* **1999**, *28*, 1474−1478.

(17) Elliott, H. A.; Dempsey, B. A. Agronomic effects of land application of water treatment sludges. *J.-Am. Water Works Assoc.* **1991**, *84*, 126−131.

(18) Novak, J. M.; Watts, D. W. Increasing the phosphorus sorption capacity of southeastern Coastal Plain soils using water treatment residuals. *Soil Sci.* **2004**, *169*, 206−214.

(19) Dayton, E. A.; Basta, N. T.; Jakober, C. A.; Hattey, J. A. Using treatment residuals to reduce phosphorus in agricultural runoff. *J.-Am. Water Works Assoc.* **2003**, *95*, 151−158.

(20) Basta, N. T.; Zupancic, R. J.; Dayton, E. A. Evaluating soil tests to predict bermudagrass growth in drinking water treatment residuals with P fertilizer. *J. Environ. Qual.* **2000**, *29*, 2007−2012.

(21) Scheidegger, A. M.; Sparks, D. L. A critical assessment of sorption−desorption mechanisms at the soil mineral/water interface. *Soil Sci.* **1996**, *161*, 813−831.

(22) Bolan, N. S.; Barrow, N. J.; Posner, A. M. Describing the effect of time on sorption of phosphate by iron and aluminium hydroxides. *J. Soil Sci.* **1985**, *36*, 187−197.

(23) Van Riemsdijk, W. H.; Lyklema, J. Reaction of phosphate with gibbsite beyond the adsorption maximum. *J. Colloid Interface Sci.* **1980**, *76*, 55−66.

(24) Nooney, M. G.; Campbell, A.; Murrell, T. S.; Lin, X. F.; Hossner, L. R.; Chusuei, C. C.; Goodman, D. W. Nucleation and growth of phosphate on metal oxide thin films. *Langmuir* **1998**, *14*, 2750−2755.

(25) Axe, L.; Trivedi, P. Intraparticle surface diffusion of metal contaminants and their attenuation in microporous amorphous Al, Fe, and Mn oxides. *J. Colloid Interface Sci.* **2002**, *247*, 259−265.

(26) Dzombak, D. A.; Morel, F. M. M. *Surface Complexation Modeling-Hydrous Ferric Oxide*; John Wiley and Sons: New York, 1990; pp 22−26.

(27) Li, L.; Stanforth, R. Distinguishing adsorption and surface precipitation of phosphate on goethite (alpha-FeOOH). *J. Colloid Interface Sci.* **2000**, *230*, 12−21.

(28) Ler, A.; Stanforth, R. Evidence for surface precipitation of phosphate on goethite. *Environ. Sci. Technol.* **2003**, *37*, 2694−2700.

(29) U.S. EPA. *Test Methods for Evaluating Solid Waste, Physical/Chemical Methods*; USEPA-65 FR 70678, Draft Update IVB SW-846; U.S. Government Printing Office: Washington, DC, 2000.

(30) McKeague, J. A.; Brydon, J. E.; Miles, N. M. Differentiation of forms of extractable iron and aluminum in soils. *Soil Sci. Soc. Am. Proc.* **1971**, *35*, 33−38.

(31) Makris, K. C. Long-term stability of sorbed phosphorus by drinking water treatment residuals: Mechanisms and implications. Ph.D. Dissertation, University of Florida, Gainesville, FL, 2004.

(32) Design-Expert. *Software for Design of Experiments*, version 6.0.5; Stat-Ease Inc.: Minneapolis, MN, 2001.

(33) Dubinin, M. M. The potential theory of adsorption of gases and vapors for adsorbents with energetically nonuniform surfaces. *Chem. Rev.* **1960**, 235−241.

(34) American Society of Civil Engineers. *Management of Water Treatment Plant Residuals*; American Society of Civil Engineers and American Water Works Association: New York and Denver, 1996.

(35) Bertrand, I.; Grignon, N.; Hinsinger, P.; Souche, G.; Jaillard, B. The use of secondary ion mass spectrometry coupled with image analysis to identify and locate chemical elements in soil minerals: the example of phosphorus. *Scanning* **2000**, *23*, 279−291.

(36) Martin, R. R.; Smart, R. S. C.; Tazaki, K. Direct observation of phosphate precipitation in the goethite/phosphate system. *Soil Sci. Soc. Am. J.* **1988**, *52*, 1492−1500.

(37) Cabrera, F.; De Arambarri, P.; Madrid, L.; Toca, G. G. Desorption of phosphorus from iron oxide in relation to pH and porosity. *Geoderma* **1981**, *26*, 203−216.

(38) Torrent, J.; Schwertmann, U.; Barron, V. Fast and slow phosphate sorption by goethite-rich natural minerals. *Clays Clay Miner.* **1992**, *40*, 14−21.

(39) Rao, J. L.; Berner, R. A. Development of an electron-microprobe method for the determination of phosphorus and associated elements in sediments. *Chem. Geol.* **1995**, *125*, 169−183.

(40) Harris, W. G.; Wang, H. D.; Reddy, K. R. Dairy manure influence on soil and sediment composition − implications for phosphorus retention. *J. Environ. Qual.* **1994**, *23*, 1071−1081.

(41) Agbenin, J. O.; Tiessen, H. Phosphorus transformations in a toposequence of lithosols and cambisols from semiarid northeastern Brazil. *Geoderma* **1994**, *62*, 345−362.

(42) Qureshi, R. H.; Jenkins, D. A.; Davies, R. I.; Rees, J. A. Application of microprobe analysis to study of phosphorus in soils. *Nature* **1969**, *221*, 1142−1147.

(43) Ippolito, J. A.; Barbarick, K. A.; Heil, D. M.; Chandler, J. P.; Redente, E. F. Phosphorus retention mechanisms of a water treatment residual. *J. Environ. Qual.* **2003**, *32*, 1857−1864.

(44) Strauss, R.; Brummer, G. W.; Barrow, N. J. Effects of crystallinity of goethite: I. Preparation and properties of goethites of differing crystallinity. *Eur. J. Soil Sci.* **1997**, *48*, 101−114.

(45) Tamura, H.; Mita, K.; Tanaka, A.; Ito, M. Mechanism of hydroxylation of metal oxide surfaces. *J. Colloid Interface Sci.* **2001**, *243*, 202−207.

(46) Vyas, S. N.; Patwardhan, S. R.; Vijayalakshimi, S.; Sri Ganesh, K. Adsorption of gases on carbon molecular sieves. *J. Colloid Interface Sci.* **1994**, *168*, 275−280.

(47) Guo, G.; Lua, A. G. Microporous activated carbons prepared from palm shell by thermal activation and their application to sulfur dioxide adsorption. *J. Colloid Interface Sci.* **2002**, *251*, 242−247.

(48) Altin, O.; Ozbelge, O.; Dogu, T. Effect of pH in an aqueous medium on the surface area, pore size, distribution, density and porosity of montmorillonite. *J. Colloid Interface Sci.* **1999**, *217*, 19−27.
(49) De Jonge, H.; Mittelmeijer-Hazeleger, M. C. Adsorption of CO_2 and N_2 on soil organic matter: nature of porosity, surface area and diffusion mechanisms. *Environ. Sci. Technol.* **1996**, *30*, 408−413.
(50) Garrido, J.; Linares-Solano, A.; Martin-Martinez, J. M.; Molina-Sabio, M.; Rodriguez-Reinoso, F.; Torregrosa, R. Use of N_2 vs CO_2 in the characterization of activated carbons. *Langmuir* **1987**, *3*, 76−81.
(51) Gregg, S. J.; Sing, K. S. W. *Adsorption, Surface Area, and Porosity*, 2nd ed.; Academic Press: London; New York, 1982.
(52) Ravikovitch, P. I.; Vishnyakov, A.; Russo, R.; Neimark, A. V. Unified approach to pore size characterization of microporous carbonaceous materials from N_2, Ar, and CO_2 adsorption isotherms. *Langmuir* **2000**, *16*, 2311−2320.
(53) Huang, W.; Schlautman, M. A.; Weber, W. J., Jr. A distributed reactivity model for sorption by soils and sediments. 5. The influence of near-surface characteristics of mineral domains. *Environ. Sci. Technol.* **1996**, *30*, 2993−3000.
(54) Xing, B.; Pignatello, J. J. Dual-mode sorption of low polarity compounds in glassy poly(vinyl chloride) and soil organic matter. *Environ. Sci. Technol.* **1997**, *31*, 792−799.
(55) Everett, D. H.; Powl, J. Adsorption in slit-like and cylindrical micropores in Henry's law region − model for microporosity of carbons *J. Chem. Soc., Faraday Trans. 1* **1976**, *72*, 619−636.
(56) Willett, I. R.; Chartres, C. J.; Nguyen, T. T. Migration of phosphate into aggregated particles of ferrihydrite. *J. Soil Sci.* **1988**, *39*, 275−282.
(57) Madrid, L.; De Arambarri, P. Adsorption of phosphate by two iron oxides in relation to their porosity. *J. Soil Sci.* **1985**, *36*, 523−530.

Received for review June 4, 2004. Revised manuscript received September 10, 2004. Accepted September 19, 2004.

ES049161J